



Cite this: *Nanoscale*, 2023, **15**, 2690

## Tunable reactivity of silver nanoclusters: a facile route to synthesize a range of bimetallic nanostructures†

Amrita Chakraborty,<sup>a</sup> Megha Maria Stanley,<sup>a</sup> Biswajit Mondal,<sup>a</sup> Nonappa,<sup>b</sup> Mohammad Bodiuzzaman,<sup>a</sup> Papri Chakraborty,<sup>a</sup> M. P. Kannan<sup>a</sup> and Thalappil Pradeep<sup>a\*</sup>

Quantized energy levels and unique optoelectronic properties of atomically precise noble metal nanoclusters (NCs) have made them important in materials science, catalysis, sensors, and biomedicine. Recent studies on the profound chemical interactions of such NCs within themselves and with ultrasmall plasmonic nanoparticles (NPs) indicate that depending on the size, shape, and composition of the second reactant, NCs can either take part in colloidal assembly without any chemical modifications or lead to products with atoms exchanged. Anisotropic NPs are a unique class of plasmonic nanomaterials as their sharp edges and protrusions show higher chemical reactivity compared to flat surfaces, often leading to site-specific growth of foreign metals and metal oxide shells. Here, using chemical interactions between gold nanotriangles (AuNTs) and Ag NCs of different compositions, we show for the first time that metal atom etching, alloying/atom exchange, and colloidal assembly can all happen at a particular length scale. Specifically, Ag<sub>25</sub>(DMBT)<sub>18</sub> NCs (denoted as **1**), upon reacting with AuNTs of ~57 nm edge length, etch gold atoms from their sharp tips and edges. Simultaneously, the two nanosystems exchange metal atoms, resulting in Ag-doped AuNTs and Au<sub>x</sub>Ag<sub>24-x</sub>(DMBT)<sub>18</sub> (x = 1, 2). However, another Ag NC with the same metallic core, but a different ligand shell, namely, Ag<sub>25</sub>H<sub>22</sub>(DPPE)<sub>8</sub> (denoted as **2**), creates dendritic shells made of Ag, surrounding these AuNTs under the same reaction conditions. Furthermore, we show that in the case of a more reactive thiol-protected Ag NC, namely, Ag<sub>44</sub>(pMBA)<sub>30</sub> (denoted as **3**), gold etching is faster from the edges and tips, which drastically alters the identities of both the reactants. Interestingly, when the AuNTs are protected by pMBA, **3** systematically assembles on AuNTs through H-bonding, resulting in an AuNT core–Ag NC shell nanocomposite. Thus, while shedding light on various factors affecting the reactivity of Ag NCs towards AuNTs, the present study proposes a single strategy to obtain a number of bimetallic nanosystems of targeted morphology and functionality.

Received 13th November 2022.

Accepted 3rd January 2023

DOI: 10.1039/d2nr06350f

[rsc.li/nanoscale](http://rsc.li/nanoscale)

## Introduction

Noble metal NCs of precise compositions and structures, composed of a few to tens of metal atoms, show molecule-like optical properties.<sup>1,2</sup> In the last decade, the synthesis of a large variety of NCs, their structural determination using single-crystal X-ray diffraction (XRD) studies, and the structure–property correlation of their physical and chemical behaviors have

been the principal aspects of research in the area, with a recent emphasis on bimetallic NCs.<sup>3–6</sup> Lately, the chemical properties of noble metal NCs are gaining attention due to their large surface to volume ratio and low coordination of surface atoms which are important for applications such as catalysis<sup>7,8</sup> and bioimaging.<sup>9</sup> Besides forming adducts with small molecules such as cyclodextrins,<sup>10,11</sup> crown ethers,<sup>12</sup> fullerenes,<sup>13</sup> and cucurbiturils,<sup>14</sup> NCs also take part in binary colloidal assemblies with 1D plasmonic NPs. For instance, pMBA capped Ag and Au NCs, when anchored to the surface of TeNWs, led them to arrange in a crossed-bilayer assembly at the liquid–air interface.<sup>15</sup> H-bonding interactions among the anchored NCs of the two layers result in precise orientations. The same NCs take part in H-bonding-mediated assemblies with pMBA-protected ultrasmall gold nanorods (AuNRs) encapsulating the latter in multilayer cages.<sup>16</sup> In such assemblies,

<sup>a</sup>Department of Chemistry, DST Unit of Nanoscience (DST UNS) and Thematic Unit of Excellence (TUE), Indian Institute of Technology Madras, Chennai 600 036, India. E-mail: [pradeep@iitm.ac.in](mailto:pradeep@iitm.ac.in)

<sup>b</sup>Faculty of Engineering and Natural Sciences, Tampere University, FI-33101 Tampere, Finland

† Electronic supplementary information (ESI) available. See DOI: <https://doi.org/10.1039/d2nr06350f>

the identities of NCs and anisotropic nanoparticles were retained. On the other hand, studies on thiol- and phosphine-protected noble metal NCs have shown that NCs of two different types of metals, when mixed under ambient conditions, spontaneously exchanged metal atoms and ligands in solution, leading to intercluster alloying.<sup>17</sup> A similar reaction between two NCs,<sup>18</sup> or NC and metal thiolates,<sup>19</sup> made of isotopically pure silver atoms resulted in isotopically mixed NCs. Bürgi and co-workers have shown that doping a different metal to Au NCs is possible by using metallic foils of Ag, Cu and Cd as the source of heteroatoms.<sup>20</sup> In a recent report, ultrasmall plasmonic Ag NPs were also found to be the source of atomic Ag while reacting with Au NCs, resulting in mono-disperse Au–Ag alloy NPs and Ag-doped Au NCs.<sup>21</sup>

These results indicate that the interaction of NCs with other nanosystems can range from weaker to strong interactive forces, either retaining<sup>16</sup> or altering their chemical properties.<sup>21</sup> Plasmonic NPs of anisotropic morphology, such as nanorods, nanobipyramids, and nanostars, show differential reactivity along their sharp protrusions, edges, and tips as compared to their flat surfaces.<sup>22–24</sup> Site-specific chemical reactivity leads to the preferential end-to-end assembly of AuNRs,<sup>25</sup> the tip-specific growth of non-metallic shells,<sup>24,26,27</sup> and the site-selective growth of foreign metals.<sup>28–30</sup> Thus, the chemical reactivity of noble metal NCs with anisotropic plasmonic NPs is an exciting field that is yet to be explored. A study by Yuan *et al.* showed that the highest curvature caused the tips of triangular gold nanoprisms to show the highest chemical reactivity followed by those of bipyramids and AuNRs.<sup>31</sup>

Therefore, we chose planar gold nanotriangles (AuNTs) as the anisotropic NPs and allowed them to interact with different Ag NCs under ambient conditions. A thorough characterization of the intermediate and product NPs reveal that the reaction with a thiolate-protected Ag NC, namely, Ag<sub>25</sub>(DMBT)<sub>18</sub> (abbreviated here as **1**), causes controlled etching of atoms from the sharp vertices and edges of AuNTs. Simultaneously, the two nanosystems exchanged metal atoms, leading to Au<sub>x</sub>Ag<sub>25–x</sub>(DMBT)<sub>18</sub> and blunt AuNTs with limited Ag doping to the surface. This unique reactivity suggests that the differential surface curvature of AuNTs makes the Au atoms at the sharp tips and edges behave like loosely bound atoms, and the flat surfaces behave like a gold foil and the heavy metallic body remains unaffected, resembling bulk gold.

We have further shown that by tuning the composition of the NC and the AuNT–Ag NC interface, the outcome of such reactions can change drastically. For example, a similar interaction of AuNTs with Ag<sub>25</sub>H<sub>22</sub>(DPPE)<sub>8</sub> (abbreviated here as **2**) produced a dendritic nanoshell of Ag surrounding the AuNTs, whereas their reaction with Ag<sub>44</sub>(pMBA)<sub>30</sub> (abbreviated here as **3**) leads to uncontrolled etching of Au atoms from the tips and edges of AuNTs. Interestingly, suitable modification of the AuNT–Ag NC interface results in a geometrically precise core–shell bimetallic nanocomposite. Thus, their chemical interaction with NCs has the potential to produce atom-etched, atom-exchanged, and core–shell products from a single nanostructure by slightly tuning the reactants and reaction parameters.

## Experimental

### Materials and methods

**Chemicals and materials.** Tetrachloroauric acid trihydrate (HAuCl<sub>4</sub>·3H<sub>2</sub>O, ≥99.9%), hexadecyltrimethylammonium chloride (CTAC, 25 wt% in water), sodium borohydride (NaBH<sub>4</sub>, ≥99%), 2,4-dimethylbenzenethiol (DMBT), 1,2-bis(diphenylphosphino)ethane (DPPE, 97%), tetraphenylbromide (PPh<sub>4</sub>Br), 4-mercaptobenzoic acid (pMBA, 97%), sodium iodide (NaI, ≥99.5%), cesium hydroxide (CsOH, >99%) and L-ascorbic acid (AA, ≥99%) were purchased from Sigma Aldrich. Silver nitrate (AgNO<sub>3</sub>, 99%) and sodium hydroxide (NaOH) pellets were obtained from Rankem, India. All analytical grade solvents, *e.g.*, *N,N*-dimethylformamide (DMF), dichloromethane (DCM), dimethyl sulfoxide (DMSO) and methanol (MeOH), were purchased from Rankem chemicals. All chemicals were used as received without further purification. Glassware was washed with aqua regia, sonicated three times with water for 3 min each, rinsed with distilled water, and dried before use. Distilled water was used for all syntheses.

**Synthesis of gold nanotriangles (AuNTs).** The seed-mediated method reported by Scarabelli *et al.* was followed to synthesize gold nanotriangles.<sup>32</sup> To prepare the seed, 25 μL of 0.05 M HAuCl<sub>4</sub> solution was added to 4.7 mL of 0.1 M CTAC solution with slow stirring. Subsequently, 0.01 M NaBH<sub>4</sub> solution was prepared in ice-cold water and 300 μL of this was injected into the reaction mixture under vigorous stirring. The seed solution was kept at 28 °C for 2 h, which was diluted 10 times using 0.1 M CTAC prior to its addition to the growth solution. For a 40 mL batch of AuNTs, the following two growth solutions were prepared.

**Growth solution A.** To 8 mL of DI water, 1.6 mL of 0.1 M CTAC, 40 μL of 0.05 M HAuCl<sub>4</sub> and 15 μL of a 0.01 M NaI solution were added sequentially under manual stirring.

**Growth solution B.** 500 μL of 0.05 M HAuCl<sub>4</sub> solution was added to 40 mL of 0.05 M CTAC, followed by 300 μL of 0.01 M NaI solution, all under manual stirring.

After the preparation of these solutions, 40 μL and 400 μL of 0.1 M AA were added to the growth solutions A and B, respectively. The reaction mixtures were manually shaken until the solution became colorless, indicating the reduction of Au(III) to Au(I). Immediately, 100 μL of the diluted seed was added to growth solution A with mild shaking. Within 1 s of this, 3.2 mL of growth solution A was added to growth solution B. The mixture was kept still for a minimum period of 1 h after the initial manual shaking for about 5 s. The appearance of a dark blue color indicated the formation of nanotriangles.

**Purification of the as-synthesized batch.** To eliminate spherical NPs formed along with the AuNTs, a flocculation method was followed, *i.e.*, a suitable amount of aqueous CTAC stock solution (25 wt%) was added to the as-synthesized AuNTs (in 5 mL batches) to achieve the final CTAC concentrations of 150, 175 and 200 mM, respectively. The mixtures were kept undisturbed overnight at 28 °C. As a result, AuNTs with better size and shape uniformity were precipitated in all

three cases while the impurities remained dispersed in the supernatant. The yield was optimum in the case of 175 mM final CTAC concentration. After decanting the supernatant, the pellets were dispersed in DI water with mild sonication, which resulted in a solution of greenish blue color.

**Synthesis of 1.** NC 1 was synthesized according to a previously reported method.<sup>33</sup> Briefly, 38 mg of AgNO<sub>3</sub> was dissolved in 2 mL of MeOH and 17 mL of DCM was added to it. Under stirring conditions, 90  $\mu$ L of 2,4-dimethylbenzenethiol (DMBT) was added to this solution. After 20 min of stirring, 6 mg of tetraphenylbromide (PPh<sub>4</sub>Br) was added followed by the addition of a freshly prepared solution of 15 mg of sodium borohydride (NaBH<sub>4</sub>) in 0.5 mL of ice-cold water. The reaction was carried out for 6 h and kept in a refrigerator (4 °C) overnight. The solvent was evaporated under reduced pressure and the product was cleaned several times with excess MeOH. The cleaned clusters were characterized by optical absorption spectroscopy and electrospray ionization mass spectrometry.

**Synthesis of 2.** NC 2 was synthesized following the procedure reported recently.<sup>34</sup> Briefly, 20 mg of AgNO<sub>3</sub> was dissolved in 5 mL of MeOH. 75 mg of DPPE dissolved in 7 mL of DCM was added to it under stirring at room temperature. Stirring was continued for 20 minutes. Meanwhile, 35 mg of NaBH<sub>4</sub> was dissolved in 1 mL of ice-cold DI water. This was added to the reaction mixture in one shot. With the addition of NaBH<sub>4</sub>, the colorless solution turned light yellow. It was crucial to carry out the synthetic procedure in the dark to avoid any undesired oxidation of Ag. After roughly 30 minutes of continuous stirring, when the reaction mixture turned orange, the product was extracted and purified to obtain clean NCs.

**Synthesis of 3.** As reported by Desireddy *et al.*,<sup>35</sup> NC 3 was synthesized by adding 128 mg of AgNO<sub>3</sub> and 173 mg of MBA to a mixture of DMSO and water (volume ratio 4 : 7) under stirring conditions. To this, an aqueous solution of CsOH (50%) was added dropwise until the solution became clear. 283 mg of NaBH<sub>4</sub> was dissolved in 9 mL of ice-cold DI water, a 1 mL aliquot of which was added dropwise to this greenish yellow clear solution at an interval of 9 minutes with continuous stirring. After this, the reaction mixture was kept under stirring conditions for 1 h to complete the reaction. As a result, the solution turned wine red, confirming the formation of 3. This crude cluster was purified in a few steps. First, it was centrifuged at 5000 rpm for 5 min to remove any NPs formed during the synthesis. Excess DMF was added to the supernatant and it was centrifuged at 5000 rpm for 1 min. To the precipitate containing 3, equal volumes of DMF and toluene were added along with citric acid. This protonated the carboxylic acid groups present in the cluster. This was centrifuged again at 5000 rpm for 1 min and the procedure was repeated once more to ensure complete protonation of the acid groups. Finally, the purified NC was dissolved in ultrapure DMF.

**Reaction between AuNTs and 1.** Purified AuNTs were subjected to centrifugation (6000 rpm for 10 min) to remove excess CTAC. 90% of the colorless supernatant was decanted

and the AuNTs settled at the bottom were redispersed in the same amount of DI water. This process was repeated once more and the pellet was finally redispersed in DMF. The concentration of the AuNT solution was maintained such that the optical density (O.D.) at the SPR maximum (~640 nm) was 1. To 500  $\mu$ L of this AuNTs, 40  $\mu$ L of purified NC 1 was added dropwise with moderate stirring at room temperature. The amount of NC added and the time of the reaction were varied for comparative studies.

**Reaction between AuNTs and 2.** In a similar way as described above, to 500  $\mu$ L of AuNTs (as above), 50  $\mu$ L of 1.2  $\mu$ g mL<sup>-1</sup> NC 2 were added under stirring conditions. The reaction was continued at room temperature.

**Reaction between AuNTs and 3.** This reaction was carried out in two ways with bare AuNTs, which was similar to the method described in the case of 1, and with *p*MBA-protected AuNTs (abbreviated as AuNT@*p*MBA). For the latter, washed AuNTs were dispersed in 500  $\mu$ L of DMF as stated above, Meanwhile, solid *p*MBA was dissolved in DMF to achieve a final concentration of 0.1 mM. 500  $\mu$ L of this was added to AuNTs and the mixture was vortexed for 10 min. After 3 h, this solution was centrifuged for 6 min at 6000 rpm and the supernatant was decanted to remove excess CTAC and unbound *p*MBA, if any. The pellet thus obtained was AuNT@*p*MBA. NC 3 was added to AuNT@*p*MBA (of O.D. 1 at 640 nm) with mild stirring, and the mixture was kept undisturbed at room temperature.

**Instrumentation.** UV-vis absorption spectra of all the samples were recorded using a PerkinElmer Lambda 25 spectrometer. A quartz cuvette of path length 10 mm was used for all measurements. TEM imaging was performed using a JEOL 3010 instrument at 200 kV acceleration voltage. For transmission electron tomographic reconstruction, the specimen was tilted between  $\pm 69^\circ$  angles with  $2^\circ$  increment and a tilt series of 2D projections were acquired with the SerialEM software package in low dose mode using a JEOL 3200 TEM operating at 300 kV with an omega filter. The acquired stack of images was subjected to a series of pre-processing, coarse alignment, and final alignment using the IMOD software package. 3D reconstruction was obtained with a custom-made maximum entropy method (MEM) program on MacPro.<sup>36</sup> STEM images were collected using a JEOL JEM 2800 microscope at 200 kV acceleration voltage. Mass spectrometric analysis was performed using a Waters Synapt G2Si high-definition mass spectrometer equipped with electrospray ionization (ESI). X-ray diffraction (XRD) patterns were recorded with a Bruker AXS D8 Discover diffractometer using Cu K $\alpha$  ( $\lambda = 1.54 \text{ \AA}$ ) radiation. Samples were scanned between the  $5^\circ$  and  $90^\circ$  range of  $2\theta$  and the peaks were matched with the JCPDS (Joint Committee on Powder Diffraction Standards) database. To identify the chemical oxidation states of the elements, XPS was performed using an ESCA probe TPD spectrometer (Omicron Nanotechnology) with a polychromatic Al K $\alpha$  ( $h\nu = 1486.6 \text{ eV}$ ) X-ray source with a step size of 0.1 eV per second. The binding energies (B.E) of all the elements were calibrated with respect to C 1s (284.8 eV).

## Results and discussion

### Interaction of AuNTs with a moderately reactive Ag NC

Equilateral AuNTs were synthesized following the synthetic methods reported by Scarabelli *et al.*,<sup>32</sup> Fig. 1a presents the TEM image of AuNTs obtained after purification by the flocculation method (Fig. S1† presents the detailed characterization). A statistical analysis of 100 AuNTs reveals that the mean particle size (distance from the tip to the opposite side) of the as-synthesized AuNTs was  $57.8 \pm 3.6$  nm (Fig. 1b). For better insight, 3D tomographic images of these AuNTs were reconstructed from the respective tilt series of TEM images. Fig. 1c and ESI Video S1† show the 3D views of AuNTs which clearly exhibit their planar triangular morphology with sharp edges and tips. Parallely, we synthesized an Ag NC that is known to exchange metal atoms with other NCs in solution,<sup>37</sup> *i.e.*, NC **1**. The synthesis of **1** was confirmed from its characteristic absorption spectrum, *i.e.*, a broad peak at  $\sim 675$  nm, an intense peak at  $\sim 490$  nm and 2 other peaks at around 336 nm and 396 nm (top panel of Fig. 1d), and ESI mass spectrum (MS) (Fig. 3a). Pristine AuNTs, protected by a labile layer of cetyl trimethyl ammonium chloride (CTAC), were dispersed in aqueous medium. After removing excess CTAC by centrifugation, the pellet of AuNTs was dispersed in DMF, which was the same solvent as **1**. A dilute solution of NC **1** was added dropwise to AuNTs under stirring conditions until the color of the medium changed from blue (characteristic color of pure AuNTs) to greenish-brown. The reaction was allowed to continue for 72 h and the product (denoted as AuNT@**1**) was separated by centrifugation for analysis. A comparison of the absorption spectra of pristine AuNTs, **1**, and AuNT@**1** presented in Fig. 1d shows that the LSPR of the AuNTs at  $\sim 630$  nm undergoes a blue shift in the latter, which can be

attributed to the reduction in the aspect ratio of the AuNTs, as often observed in the case of conventional oxidative etching.<sup>31</sup> Peaks between 350 nm and 450 nm come from unreacted **1** adsorbed on the surface of the AuNTs. The increased width of all the peaks denotes electronic coupling between the two systems. The broad peak around 800 nm is presumably due to the quantum mechanical effect as explained by Lahtinen *et al.* in the case of Au<sub>250</sub> trimers.<sup>38</sup> The TEM image of the reacted AuNTs in Fig. 1e confirms that the morphology of the AuNTs was significantly altered upon reaction. The particles retained their triangular shape, but the edges were rounded and the tips were blunt. The particle size distribution of AuNT@**1** in Fig. 1f indicates that the average size of the NTs has been reduced by 12 nm and the size-polydispersity has increased. Fig. 1g (also ESI Video S2†) presents the electron tomographic 3D reconstruction of AuNT@**1** particles that gives a better insight on the overall pebble-like morphology. We must clarify that the label, AuNT@**1**, does not imply that **1** is covering AuNTs. We also note that gold atoms can migrate from the sharp tips of AuNTs to their flat surfaces when dispersed in DI water.<sup>39</sup> However, the TEM images of AuNTs dispersed in DMF show that even after a week there was no alteration in the geometry of the AuNTs (Fig. S2†).

To study the gradual change of AuNTs during the reaction, the reaction product was extracted at different time intervals and their TEM and STEM images were examined carefully. In Fig. 2a, the TEM image of AuNT@**1** after 24 hours of the reaction showed a hint of bulging along the flat sides of the particles. This image implies that metallophilic attraction led **1** to attach to the AuNTs, preferentially on their planar surfaces, which exerted stronger van der Waals force compared to their edges. Such adducts were also formed at the intermediate stages of the reaction between polydisperse AgNPs and Au

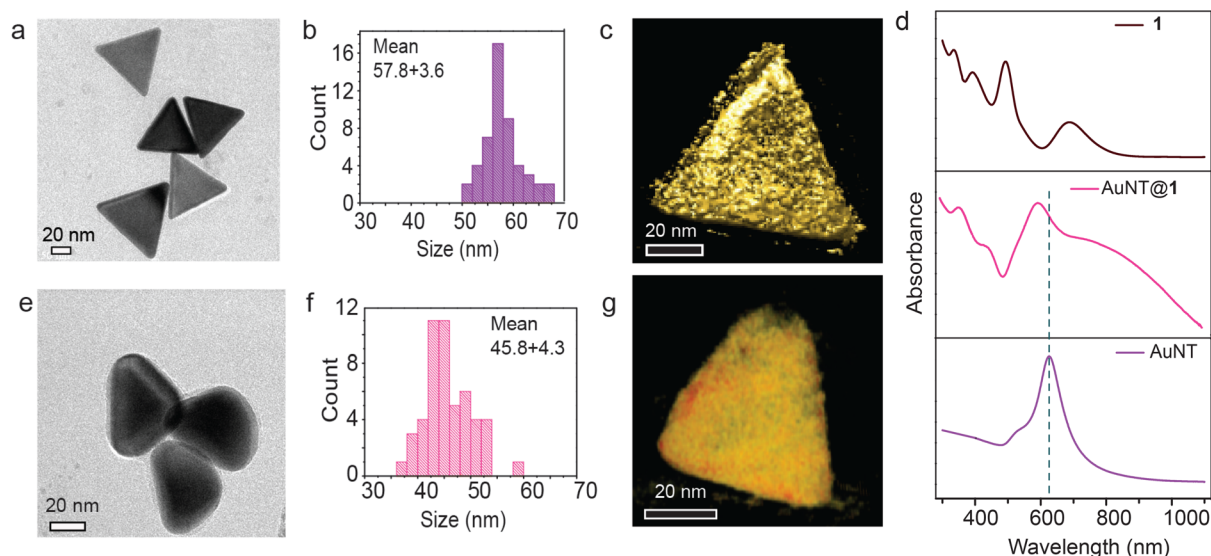


**Fig. 1** Characterization of AuNTs before and after the reaction with **1**: (a) TEM image of parent AuNTs and (b) the corresponding particle size distribution, (c) 3D tomographic reconstruction of a single AuNT, (d) comparative absorption spectra of **1**, AuNT@**1**, and AuNTs, (e) TEM image of AuNT@**1**, (f) the corresponding particle size distribution and (g) 3D tomographic reconstruction of a single AuNT@**1**.

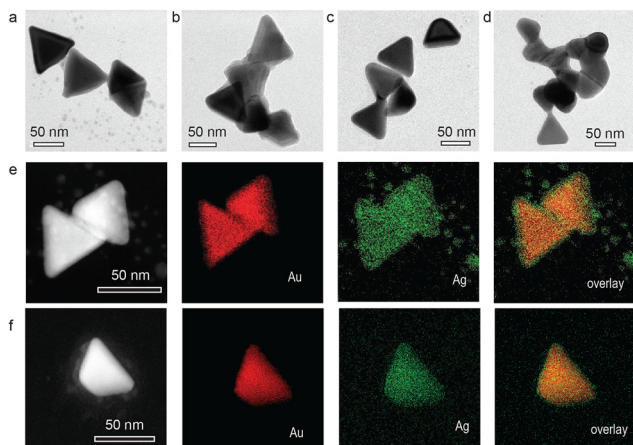


**Fig. 2** Time-dependent analysis of AuNT@1: TEM images of the reaction product after (a) 1 day, (b) 3 days, (c) 6 days and (d) 10 days. (e) STEM EDS elemental mapping of AuNT@1 after 3 days of the reaction, and (f) after 6 days of the reaction.

NCs, as observed by Bose *et al.*<sup>21</sup> In the present study, after 72 h of the reaction, more cluster moieties got adsorbed on AuNTs forming AuNT-1 adducts, as shown in Fig. 2b. At this stage, the tips of the nanotriangles started to lose their sharpness, suggesting the etching of Au atoms from the highly curved and least protected (by CTAC) surfaces of the AuNTs upon reaction. Fig. 2c presents the TEM image of AuNT@1 after 6 days, which shows that the AuNTs became blunt. In the case of the oxidative etching of anisotropic Au NPs, we have seen that the rate of reshaping decreases significantly with time as the surface curvature increases.<sup>31</sup> Accordingly, the TEM image of AuNT@1 taken after 10 days of reaction (Fig. 2d) suggests that, after a certain point, the reshaping of AuNTs was ceased. Although a prolonged reaction time removed CTAC from the surface of AuNTs, causing them to fuse with each other, most of the reacted AuNTs still carried the signature of their triangular morphology. The rate of the reaction and end results were hardly affected by an increase in the NC concentration in the reaction medium (Fig. S3†).

STEM EDS elemental mapping of the reacted particles was also performed at the two significant stages of the transformation. Fig. 2e represents a dark-field STEM image of AuNT@1 and the corresponding EDS elemental mapping after 72 h of the reaction. At this intermediate stage, a thin non-uniform Ag shell surrounding the sharp AuNTs can be observed along with some unreacted NC in the vicinity. The STEM image of such a single particle collected after 6 days of reaction (Fig. 2f) shows that besides the vertices, the edges of the particles also lost their sharpness, thereby destroying the planar geometry of the parent AuNTs. Besides, the particle seemed to be free from any loosely bound NC. However, the corresponding EDS elemental mapping shows that Ag was evenly distributed on the surface of the reacted AuNTs, but no trace of S was found, suggesting the absence of DMBT. This observation confirms that there was no reacted or unreacted NC adsorbed on the

AuNT surface, rather elemental Ag was doped to the AuNTs in a metal exchange reaction.

We then performed powder XRD analysis, which showed no change in the lattice spacing of the AuNTs upon reaction (Fig. S4†). Together, these two studies indicate that Ag atoms were doped to the AuNTs, but the doping of Ag atoms was limited to the surface and didn't result in alloying of the whole body of nanotriangles.

Plasmonic nanoparticles such as AuNTs are not atomically precise. Even the best synthetic batch of AuNTs do not all contain the same number of Au atoms. Hence, chances are that the number of Ag atoms doped to AuNTs will vary. Mass spectrometric analysis of the change of AuNTs is beyond the limit of commercially available mass spectrometers. Hence, a definite value of Ag atoms doped per AuNT is hard to determine. However, NCs are ultrasmall, atomically precise structures. Hence, the reacted NC was analyzed using ESI MS in order to comprehend the mechanistic pathway. Precisely, after 72 h of the reaction, the solution was centrifuged to spin down the AuNT@1 particles and the supernatant was analyzed. The ESI MS of **1** before and after reaction are shown in Fig. 3a. The intense peak at  $m/z \sim 5167$  in both the cases is attributed to the molecular ion peak with a molecular formula of  $[\text{Ag}_{25}(\text{DMBT})_{18}]^-$ . In case of the reacted NC, the appearance of a new peak at  $m/z \sim 5256$  indicates that an Ag atom of some of the NCs was replaced with an Au atom. Another weak signal found at  $m/z \sim 5345$  corresponds to the replacement of 2 Ag atoms of **1** by 2 Au atoms, keeping the nuclearity constant, namely,  $[\text{Ag}_{25-x}\text{Au}_x(\text{DMBT})_{18}]^-$  ( $x = 1, 2$ ). This is direct evidence of atom exchange between AuNTs and **1**, resembling a chemical reaction. Along with the atom exchange products, we observed two intense peaks at  $m/z \sim 4923$  and  $\sim 4679$ , which are due to the loss of one and two (Ag-DMBT) units, respectively from the parent NC. However, these (Ag-DMBT)<sub>n</sub>-deficient NC moieties showed no trace of Au doping, suggesting that atom-etched NC moieties did not take part in atom exchange

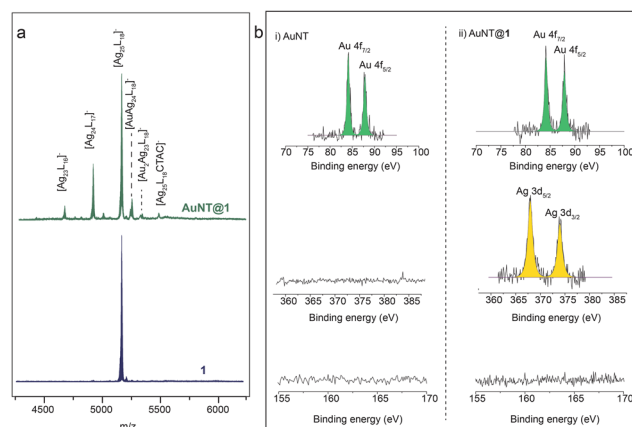


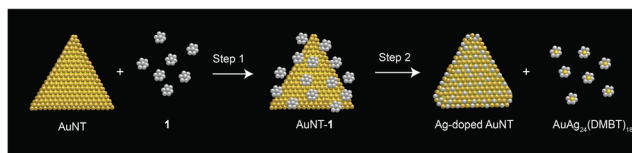
**Fig. 3** (a) ESI MS study of **1** before and after the reaction with AuNTs, (b) comparative XPS analysis showing the emergence of an Ag peak in AuNT@1, but no signal was seen around 162 eV denoting the absence of S.

with AuNTs and *vice versa*. These may also be a result of the fragmentation of **1** during the reaction. The X-ray photoelectron spectroscopic study of parent AuNTs and AuNT@**1** reveals the presence of Ag in the latter; however, no trace of S was found (Fig. 3b). The above results reconfirm that metallic Ag was incorporated to AuNTs in its elemental form and not in the form of the adsorbed Ag-DMBT unit or unreacted **1** as that would produce a signal for S as well. Based on these observations and the previous studies of chemical interactions between nanosystems, we propose a mechanism of the reaction between bare AuNTs and **1**. Krishnadas *et al.* have shown that the reaction between Au and Ag NCs leads to atom exchange products even up to the complete conversion of one metal cluster to the other, one atom at a time.<sup>37</sup> Even small AgNPs, due to the high surface to volume ratio, are known to show profound reactivity towards Au NCs. Such reactivity between plasmonic NPs and NCs decreased significantly upon increasing the size of AgNPs from 4 nm to 8 nm.<sup>21</sup> Hence, considering their dimension, AuNTs are not expected to take part in atom exchange with Ag NCs to a significant extent. However, due to their non-spherical morphology, Au atoms along their edges and tips took part in the reaction.

As expected from the previous reports of chemical reactions among nanosystems, an AuNT-**1** adduct was formed in step 1 of the reaction due to the metallophilic attraction between the reactants. Now, Au atoms at the sharp edges and vertices of AuNTs were under-coordinated, and hence, more exposed to the reactant NC (here, **1**). In step 2, loosely bound Au atoms leached out from the vertices and edges of the sharp AuNTs converting the latter into blunt pebble-like triangular NPs. On the other hand, some of the NCs lost Ag-DMBT units from their inherent composition. Such a partial decomposition of NCs to form metal thiolates was observed earlier in the presence of a foreign metal ion.<sup>40</sup> In a parallel pathway, the AuNTs and undecomposed **1** moieties exchange metal atoms, producing Ag@AuNTs and  $[\text{Ag}_{25-x}\text{Au}_x(\text{DMBT})_{18}]^-$  ( $x = 1, 2$ ). Thus, the reaction simultaneously produces Au-doped Ag NCs and Ag-doped AuNPs as the end products. Scheme 1 shows the overall reaction between AuNTs and **1**. Notably, although ligand exchange is quite a common phenomenon of NC reactivity,<sup>41</sup> in this case we observed only metal atom transfer to the AuNTs and no ligand exchange.

### Effect of the shell of the NC

The physical and chemical properties of noble metal NCs are guided by their atomic composition, the nature of the ligand, and the structure of the metallic core.<sup>1</sup> Therefore, to have a



Scheme 1 Two-step reaction between AuNTs and **1**.

complete understanding of the chemical reactivity of NCs with anisotropic NPs, it is crucial to study the effect of these parameters. In order to investigate the effect of the ligand shell in the present reaction, we synthesized another Ag NC of the same metallic core as **1**, but the protecting shell is made of a phosphine ligand instead of a thiol.<sup>34</sup> This NC, namely, **2** was soluble in methanol, whereas AuNTs were dispersed in DI water. The clear blue aqueous dispersion of AuNTs turned turbid instantly as **2** was added to it with moderate stirring. This indicates that the DPPE ligands came out of the NC, partially or fully, into the reaction medium. The absorption spectrum of the reaction product, namely, AuNT@**2** showed no significant shift in the LSPR peak position even after 6 days of the reaction (Fig. 4a). TEM images collected after 1 day (Fig. 4b) and 6 days (Fig. 4c) of the reaction showed that the reaction with **2** did not affect the size and aspect ratio of AuNTs in aqueous medium. In the EDS elemental analysis of AuNT@**2**, an intense signal for Au and Ag was obtained, but no trace of P was found (Fig. S5†). This was possibly because in aqueous medium, the ligand of **2** precipitated, decomposing the NC too soon to effectively react with AuNTs and alter their morphology. However, the naked core of **2** acted as a source of Ag(0) that was doped to the surface of AuNTs. As a result, even after days of the reaction, the vertices and edges of AuNTs were sharp, retaining their planar geometry. The inset of Fig. 4c presents the respective particle size distribution, which closely matches that of the average size of parent AuNTs.

### Effect of solvent on the reaction product

The solvent often plays a crucial role in weak chemical interactions among nano-systems. DMF has been widely used as the medium of nanoscale reactions in earlier studies<sup>17</sup> and in case of the reaction between AuNTs and **1**. Interestingly, in

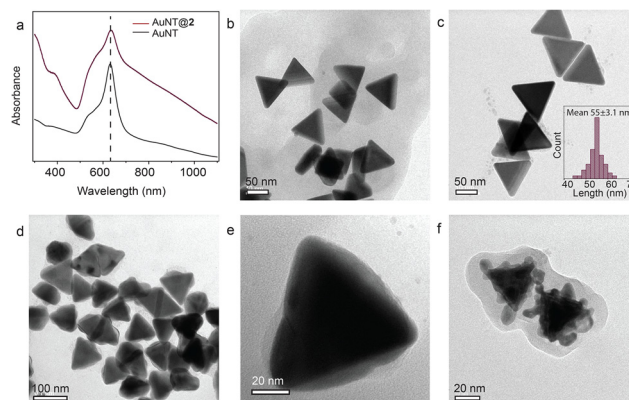


Fig. 4 Characterization of AuNT@**2**: (a) comparative absorption spectra of AuNTs before and after the reaction with **2** in water (vertically translated for a clear view) and (b) TEM images of AuNT@**2** after 1 day and (c) after 6 days, with the corresponding particle size distribution in the inset. (d) TEM image of AuNT@**2**-DMF, (e) magnified view of a single AuNT@**2**-DMF particle, and (f) TEM image of AuNT@**2**-DMF upon reacting with an excess amount of **2**.

DMF, **2** reacts with AuNTs in a very different way than in aqueous medium. The reaction product, abbreviated as AuNT@2-DMF, showed a non-uniform over-growth on the flat surfaces of AuNTs, as evident from their TEM images (Fig. 4d and e). Respective EDS analysis of this structure showed traces of Ag, indicating the doping of Ag to AuNTs. With increasing NC concentration (2.5 times), the thickness of irregularly deposited Ag was increased. An additional thin layer of Ag was also observed surrounding these hybrid structures in the respective TEM image (Fig. 4f). The absence of P in the TEM EDS studies of these structures (Fig. S6†) proves that the nodules are made of elemental Ag, and not of unreacted or partially decomposed **2**. Since the metallic core of **2** was the same as **1**, and the solvent was the same in both the cases, this difference in reactivity was directly related to the different surface ligands of the NCs. Phosphine-protected Au NCs are known to undergo ligand exchange by reaction with thiols or metal thiolates,<sup>42</sup> which implies that phosphines are much more labile as ligands compared to thiols. In **2**, the core is protected by labile hydride and DPPE ligands, making them highly reactive. However, crystallization of **1** has been possible,<sup>33</sup> showing their greater stability. This is aligned with our observation that under the reaction conditions (especially the solvent), NC **2** decomposed and Ag atoms were doped to the AuNTs, while NC **1** exchanged Ag-DMBT units with them. Furthermore, while water stabilizes elemental Ag, and thereby hinders the chemical interaction between the two nano-systems, less polar solvents such as DMF facilitate it.

### Effect of the atomicity of the NC core

In the previous studies of intercluster reactions, Au<sub>25</sub>(PET) is known to exchange metal atoms with Ag NCs of different atomicity to different extents.<sup>17</sup> Therefore, we synthesized **3** following an established protocol.<sup>35</sup> The synthesis was verified by the characteristic absorption features (Fig. 5a) and ESI MS of the NC (Fig. S7a†) before it was added to AuNTs dispersed in DMF with continuous stirring. Initially, the color of the NC disappeared instantly upon addition, suggesting a fast chemical interaction. Dropwise addition of **3** continued until the

characteristic wine-red color of **3** was persistent in the reaction mixture. By comparing the absorption spectra of **3**, the reaction product (denoted as AuNT@**3**) and AuNTs, we observed that the LSPR peak of AuNTs was blue-shifted and significantly broadened while the signature peaks of the NC were not distinctly visible (Fig. 5a). TEM images of AuNT@**3** after 0, 1, 3 and 6 days are presented in Fig. 5b–e, which show that in the case of **3**, Au atoms continued to etch from the tips of AuNTs until the triangular morphology of the particles was lost completely. Due to this fast and uncontrolled reaction, the molecular ion peak of **3** disappeared and the corresponding Au-doped Ag NC was not detected in ESI MS analysis (Fig. S7a†). Instead, red-luminescent by-products were obtained (Fig. S7b and c†), which presumably were mixed metal thiolates, that are known to show aggregation-induced luminescence.<sup>43</sup>

### Effect of the surface ligand of the AuNTs

The as-synthesized AuNTs were stabilized by CTAC through a non-covalent interaction. From flat sides to edges to the vertices of AuNTs, as the curvature of the surface increases, the extent of surface coverage by CTAC molecules is lower. This makes the Au atoms at the sharp tips more accessible to the reactant NCs, which came out from the AuNTs during the course of the reaction with **1** and **3**. Now, AuNPs can be easily and efficiently functionalized with different thiol molecules by Au–S bond formation.<sup>44</sup> In a previous report, we have seen that pMBA-functionalization of AuNRs allowed them to act as a template for the systematic multi-layer assembly of **3** surrounding them.<sup>16</sup> Here, in order to explore the role of the AuNT–Ag NC interface on their chemical interaction, the CTAC layer of AuNTs was replaced with the respective ligands (DMBT and pMBA) *via* the ligand exchange method (see the Experimental methods section) prior to the reaction with **1** and **3**. Choosing the same ligand as that of the reactant NC was important to avoid the formation of complex by-products. The functionalization was verified by TEM EDS elemental analysis and Raman spectroscopic studies (Fig. S8 and S9†). TEM images revealed that even after 10 days of the reaction with **1**, DMBT-protected AuNTs suffered little or no morphological changes (Fig. S8c†), presumably because DMBT molecules hindered the necessary collision between the surface Au atoms and Ag NCs. The ESI MS spectra of the reacted NC showed no additional peak in this case, suggesting that the surface protection refrained the AuNTs to take part in atom exchange chemistry with **1**. However, in the case of pMBA functionalization, AuNTs interacted with **3** in a very different way. **3** is known to take part in the inter- and intrasystem H-bonding through their ligand shell.<sup>45</sup> Since the pMBA molecules bind to the AuNTs *via* the Au–S covalent bond, their –COOH groups were available for H-bond formation. As expected from their interaction with pMBA-protected AuNRs reported previously,<sup>16</sup> **3** took part in the H-bonding mediated assembly to produce a multilayer shell surrounding the AuNTs, completely encapsulating individual AuNT@pMBA. Fig. 6a shows the proposed scheme. The TEM image of the resulting nanostructure, named, AuNT@pMBA@**3**, reveals their core-shell geometry (Fig. 6b),

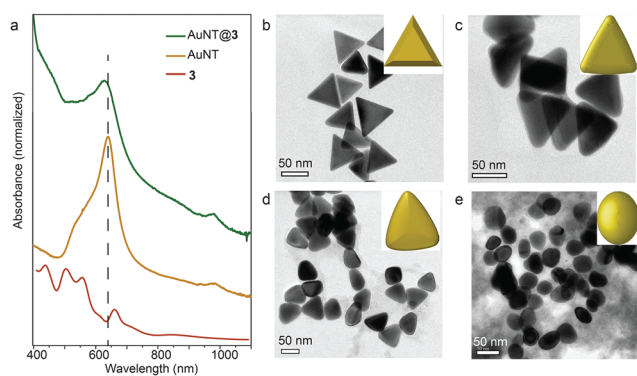


**Fig. 5** Characterization of AuNT@**3**: (a) UV-vis absorption spectra of **3**, AuNTs and AuNT@**3**, and TEM images of AuNT@**3** after (b) 0 day, (c) 1 day, (d) 3 days and (e) 6 days of the reaction.

where the shell follows the morphology of the underlying AuNTs. However, the thickness of the shells was not strictly uniform. AuNT@pMBA that was well-isolated from the neighboring particles, allowed more layers of 3 NCs to grow surrounding it (Fig. 6c), as compared to the aggregated ones (Fig. 6b). Thus, while in every other case the chemical interaction with Ag NCs led to atom exchange or removal or both, here the two nanosystems assembled through H-bonds between the ligand shells. The absorption spectrum of the product composite contained the signature peaks of both AuNTs and 3 (Fig. 6d), suggesting that the parent NC retained their identity in this hybrid nanostructure.

A red shift of the LSPR peak as compared with that of AuNT@pMBA suggests an increase in the effective edge-length due to the coupling with 3 in the core-shell structure. The FESEM image of AuNT@pMBA@3 and the corresponding EDS elemental analysis are presented in Fig. S10.† The line profile (Fig. S10b†) shows the distribution of elemental Au, Ag and S along a single particle. Fig. S10c and S10d† (corresponding to points denoted as 1 and 2, respectively) show that at the centre, the particle contains ~62% Au and ~20% Ag, whereas the edge contained ~22% Au and ~52% Ag. However, the amount of S at point 2 is lesser than expected from the composition of 3, which can be attributed to beam-induced damage

caused to the NC shell. While AuNT@1, AuNT@2 and AuNT@3 showed insignificant morphological or compositional changes, the TEM image of AuNT@pMBA@3 collected after 2 months (Fig. 6e) shows that the AuNTs retained their morphology perfectly in the composite, while the uniform shell was turned into 'islands' or 'nodules'. This can be because the pMBA ligands attached to the surface of AuNTs prevented the stronger chemical interaction between 3 and the underlying AuNTs, keeping the morphology of the encapsulated AuNTs intact. However, ultrafine NCs such as 3, consisting of a few metal atoms, possess an extremely high surface energy, and are prone to aggregation. Studies have shown that Ag NCs, anchored to the surfaces such as graphite,<sup>46</sup> TeNWs,<sup>47</sup> etc., start to diffuse, presumably to reduce the interfacial energy (between the NC and the planar surface). During such mobility, the NCs encounter adjacent NC moieties, and coalesce to produce aggregates. This result is particularly interesting as significant effort has been made into growing Au,<sup>48</sup> Ag,<sup>50</sup> or Au-Ag bimetallic islands<sup>49</sup> on anisotropic Au NPs previously to achieve promising candidates for SERS-based studies. However, there are limited reports on the wet chemical synthesis in this direction. Our present strategy of a straightforward colloidal assembly produces an AuNT core-Ag island nanostructure spontaneously with time.

## Conclusions

In conclusion, we have shown that due to differential surface energies, gold atoms at the tips, flat surfaces, and core of a single anisotropic nanoparticle, namely, AuNT, interact with atomically precise Ag NCs to various extents. Parallely, the low-coordinated atoms are etched from the sharp tips of the AuNTs, and Ag atoms are doped to their surface, while the core of the AuNTs is unaltered. Moreover, a series of anisotropic Au core-Ag shell nanostructures were achieved by tuning the compositions of the Ag NC, solvent, and AuNT-Ag NC interface. Thus, our present study reflects the versatile nature of nanoscale reactivity and explores its sensitivity towards some of the factors such as the surface curvature, solvent, and surface protective layer, leaving a scope to explore further. For example, the effect of size of the nanotriangle on such reactivity with silver nanoclusters will be an interesting follow-up study. Such bimetallic anisotropic core-shell and alloy nanostructures play promising roles in diverse applications and therefore, a common strategy to synthesize them at room temperature has immense importance in the field of materials science. Thus, while exploring the chemical properties of noble metal NCs, the present study shows their utility in creating advanced nanostructures of desired functionalities.

## Conflicts of interest

The authors declare no conflicts of interest.

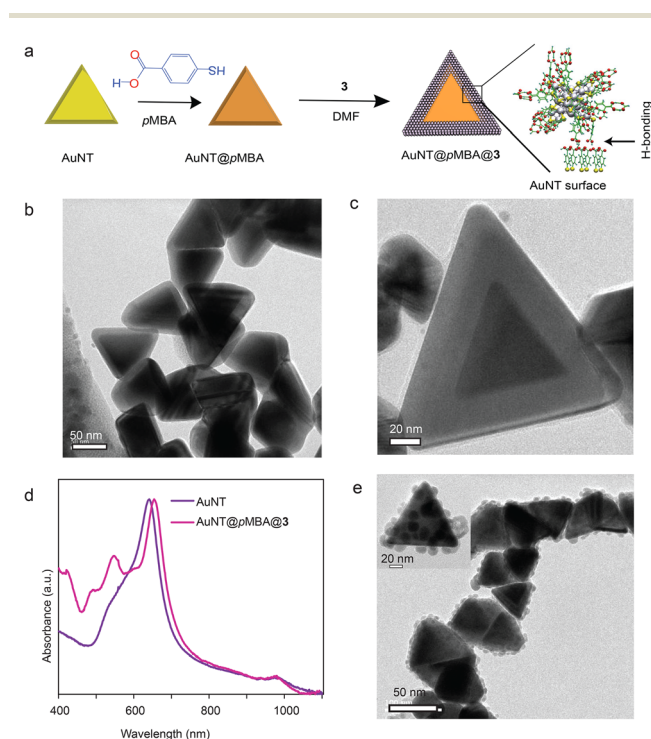


**Fig. 6** Interaction between AuNT@pMBA and 3: (a) schematic representation of the H-bond mediated assembly of 3 on the AuNT@pMBA template, (b) TEM image of AuNT@pMBA@3 after 24 h, (c) that of a single AuNT@pMBA@3 clearly showing the core-shell composite structure, (d) UV-vis absorption spectra of AuNT and AuNT@pMBA@3, and (e) TEM image of AuNT@pMBA@3 after 2 months, the inset shows that of a single particle.

## Acknowledgements

We thank the Department of Science and Technology, Government of India for constantly supporting our research program. A. C. thanks CSIR for her senior research fellowship. M. M. S. thanks Department of Chemistry, Stella Maris College, Chennai and INSA-IASc-NASI Summer Research Fellowship. We also thank the Academy of Finland for project funding (BioBase, No. 352900), Photonics Research and Innovation (PREIN) flagship and Nanomicroscopy Centre at Aalto University for access to instrumentation facilities. M. P. K. thanks MRF and B. M., M. B., P. C., and S. B. thank IIT Madras for their research fellowships.

## References

- I. Chakraborty and T. Pradeep, *Chem. Rev.*, 2017, **117**, 8208–8271.
- Atomically Precise Metal Nanoclusters*, ed. T. Pradeep, Elsevier, Amsterdam, 2023.
- Z. Wang, R. Senanayake, C. M. Aikens, W.-M. Chen, C.-H. Tung and D. Sun, *Nanoscale*, 2016, **8**, 18905–18911.
- B.-L. Han, Z. Wang, R. K. Gupta, L. Feng, S. Wang, M. Kurmoo, Z.-Y. Gao, S. Schein, C.-H. Tung and D. Sun, *ACS Nano*, 2021, **15**, 8733–8741.
- Y. Yang, T. Jia, Y.-Z. Han, Z.-A. Nan, S.-F. Yuan, F.-L. Yang and D. Sun, *Angew. Chem., Int. Ed.*, 2019, **58**, 12280–12285.
- L. Tang, A. Ma, C. Zhang, X. Liu, R. Jin and S. Wang, *Angew. Chem., Int. Ed.*, 2021, **60**, 17969–17973.
- Y. Du, H. Sheng, D. Astruc and M. Zhu, *Chem. Rev.*, 2020, **120**, 526–622.
- S. Yamazoe, K. Koyasu and T. Tsukuda, *Acc. Chem. Res.*, 2014, **47**, 816–824.
- Nonappa, *Beilstein J. Nanotechnol.*, 2020, **11**, 533–546.
- A. Mathew, G. Natarajan, L. Lehtovaara, H. Häkkinen, R. M. Kumar, V. Subramanian, A. Jaleel and T. Pradeep, *ACS Nano*, 2014, **8**, 139–152.
- A. Nag, P. Chakraborty, G. Paramasivam, M. Bodiuzzaman, G. Natarajan and T. Pradeep, *J. Am. Chem. Soc.*, 2018, **140**, 13590–13593.
- P. Chakraborty, A. Nag, K. S. Sugi, T. Ahuja, B. Varghese and T. Pradeep, *ACS Mater. Lett.*, 2019, **1**, 534–540.
- P. Chakraborty, A. Nag, B. Mondal, E. Khatun, G. Paramasivam and T. Pradeep, *J. Phys. Chem. C*, 2020, **124**, 14891–14900.
- T. Jiang, G. Qu, J. Wang, X. Ma and H. Tian, *Chem. Sci.*, 2020, **11**, 3531–3537.
- A. Som, I. Chakraborty, T. A. Maark, S. Bhat and T. Pradeep, *Adv. Mater.*, 2016, **28**, 2827–2833.
- A. Chakraborty, A. C. Fernandez, A. Som, B. Mondal, G. Natarajan, G. Paramasivam, T. Lahtinen, H. Häkkinen, Nonappa and T. Pradeep, *Angew. Chem., Int. Ed.*, 2018, **57**, 6522–6526.
- K. R. Krishnadas, A. Baksi, A. Ghosh, G. Natarajan, A. Som and T. Pradeep, *Acc. Chem. Res.*, 2017, **50**, 1988–1996.
- P. Chakraborty, A. Nag, G. Natarajan, N. Bandyopadhyay, G. Paramasivam, M. K. Panwar, J. Chakrabarti and T. Pradeep, *Sci. Adv.*, 2019, **5**, eaau7555.
- L. Tang, X. Kang, X. Wang, X. Zhang, X. Yuan and S. Wang, *Inorg. Chem.*, 2021, **60**, 3037–3045.
- R. Kazan, U. Müller and T. Bürgi, *Nanoscale*, 2019, **11**, 2938–2945.
- P. Bose, P. Chakraborty, J. S. Mohanty, Nonappa, A. Ray Chowdhuri, E. Khatun, T. Ahuja, A. Mahendranath and T. Pradeep, *Nanoscale*, 2020, **12**, 22116–22128.
- X. Zhuo, X. Zhu, Q. Li, Z. Yang and J. Wang, *ACS Nano*, 2015, **9**, 7523–7535.
- W. Zhang, J. Liu, W. Niu, H. Yan, X. Lu and B. Liu, *ACS Appl. Mater. Interfaces*, 2018, **10**, 14850–14856.
- B. Wu, D. Liu, S. Mubeen, T. T. Chuong, M. Moskovits and G. D. Stucky, *J. Am. Chem. Soc.*, 2016, **138**, 1114–1117.
- J. Wu, Y. Xu, D. Li, X. Ma and H. Tian, *Chem. Commun.*, 2017, **53**, 4577–4580.
- H. Jia, A. Du, H. Zhang, J. Yang, R. Jiang, J. Wang and C.-y. Zhang, *J. Am. Chem. Soc.*, 2019, **141**, 5083–5086.
- A. Kim, S. Zhou, L. Yao, S. Ni, B. Luo, C. E. Sing and Q. Chen, *J. Am. Chem. Soc.*, 2019, **141**, 11796–11800.
- F. Wang, S. Cheng, Z. Bao and J. Wang, *Angew. Chem., Int. Ed.*, 2013, **52**, 10344–10348.
- X. Zhu, H. Jia, X.-M. Zhu, S. Cheng, X. Zhuo, F. Qin, Z. Yang and J. Wang, *Adv. Funct. Mater.*, 2017, **27**, 1700016.
- Y. Li, H. Lin, W. Zhou, L. Sun, D. Samanta and C. A. Mirkin, *Sci. Adv.*, 2021, **7**, eabf1410.
- H. Yuan, K. P. F. Janssen, T. Franklin, G. Lu, L. Su, X. Gu, H. Uji-i, M. B. J. Roeloffs and J. Hofkens, *RSC Adv.*, 2015, **5**, 6829–6833.
- L. Scarabelli, M. Coronado-Puchau, J. J. Giner-Casares, J. Langer and L. M. Liz-Marzán, *ACS Nano*, 2014, **8**, 5833–5842.
- C. P. Joshi, M. S. Bootharaju, M. J. Alhilaly and O. M. Bakr, *J. Am. Chem. Soc.*, 2015, **137**, 11578–11581.
- M. Jash, A. C. Reber, A. Ghosh, D. Sarkar, M. Bodiuzzaman, P. Basuri, A. Baksi, S. N. Khanna and T. Pradeep, *Nanoscale*, 2018, **10**, 15714–15722.
- A. Desiredy, B. E. Conn, J. Guo, B. Yoon, R. N. Barnett, B. M. Monahan, K. Kirschbaum, W. P. Griffith, R. L. Whetten, U. Landman and T. P. Bigioni, *Nature*, 2013, **501**, 399–402.
- P. Engelhardt, in *Electron Microscopy: Methods and Protocols*, ed. J. Kuo, Humana Press, Totowa, NJ, 2007, pp. 365–385, DOI: [10.1007/978-1-59745-294-6\\_18](https://doi.org/10.1007/978-1-59745-294-6_18).
- K. R. Krishnadas, D. Ghosh, A. Ghosh, G. Natarajan and T. Pradeep, *J. Phys. Chem. C*, 2017, **121**, 23224–23232.
- T. Lahtinen, E. Hulkko, K. Sokołowska, T.-R. Tero, V. Saarnio, J. Lindgren, M. Pettersson, H. Häkkinen and L. Lehtovaara, *Nanoscale*, 2016, **8**, 18665–18674.
- F. Qin, T. Zhao, R. Jiang, N. Jiang, Q. Ruan, J. Wang, L.-D. Sun, C.-H. Yan and H.-Q. Lin, *Adv. Opt. Mater.*, 2016, **4**, 76–85.
- M. A. Habeeb Muhammed and T. Pradeep, *Chem. Phys. Lett.*, 2007, **449**, 186–190.

- 41 Y. Wang and T. Bürgi, *Nanoscale Adv.*, 2021, **3**, 2710–2727.
- 42 G. H. Woehrle, L. O. Brown and J. E. Hutchison, *J. Am. Chem. Soc.*, 2005, **127**, 2172–2183.
- 43 D. Bain, S. Maity and A. Patra, *Chem. Commun.*, 2020, **56**, 9292–9295.
- 44 M. R. Dewi, G. Laufersky and T. Nann, *RSC Adv.*, 2014, **4**, 34217–34220.
- 45 B. Yoon, W. D. Luedtke, R. N. Barnett, J. Gao, A. Desireddy, B. E. Conn, T. Bigioni and U. Landman, *Nat. Mater.*, 2014, **13**, 807–811.
- 46 I. M. Goldby, L. Kuipers, B. von Issendorff and R. E. Palmer, *Appl. Phys. Lett.*, 1996, **69**, 2819–2821.
- 47 A. Som, A. K. Samal, T. Udayabhaskararao, M. S. Bootharaju and T. Pradeep, *Chem. Mater.*, 2014, **26**, 3049–3056.
- 48 G. Wang, Y. Liu, C. Gao, L. Guo, M. Chi, K. Ijio, M. Maeda and Y. Yin, *Chem*, 2017, **3**, 678–690.
- 49 Q. Fan, K. Liu, J. Feng, F. Wang, Z. Liu, M. Liu, Y. Yin and C. Gao, *Adv. Funct. Mater.*, 2018, **28**, 1803199.
- 50 L. Chen, R. Li and P. Yang, Plasmonic nanoprobe based on the shape transition of Au/Ag core-shell nanorods to dumbbells for sensitive Hg-ion detection, *RSC Advances*, 2019, **9**, 17783–17790.